AIP | Journal of Applied Physics

Structural, electronic, optical, and magneto-optical properties of Bi12MO20 (M=Ti, Ge, Si) sillenite crystals from first principles calculations

A. F. Lima, S. A. S. Farias, and M. V. Lalic

Citation: J. Appl. Phys. **110**, 083705 (2011); doi: 10.1063/1.3652751
View online: http://dx.doi.org/10.1063/1.3652751
View Table of Contents: http://jap.aip.org/resource/1/JAPIAU/v110/i8
Published by the AIP Publishing LLC.

Structural, electronic, optical, and magneto-optical properties of $Bi_{12}MO_{20}$ (M = Ti, Ge, Si) sillenite crystals from first principles calculations

A. F. Lima,[1] S. A. S. Farias,[2] and M. V. Lalic[2,a)]
[1]*Universidade Federal de Sergipe, Departamento de Física do Campus de Itabaiana, Itabaiana/SE 49500-000, Brazil*
[2]*Universidade Federal de Sergipe, Departamento de Física, P. O. Box 353, São Cristóvão/SE 49100-000, Brazil*

(Received 3 July 2011; accepted 1 September 2011; published online 20 October 2011)

The structural, electronic, optical, and magneto-optical properties of the three $Bi_{12}MO_{20}$ sillenites (BMO; M = Ti, Ge, and Si) have been investigated on the basis of the first-principles calculations performed by the full potential augmented plane wave method. The BMO's linear optical responses are found to be very similar, but their optical rotatory powers and Faraday ellipticities exhibit notable differences in both visible and ultraviolet parts of the spectra. These differences originate from the subtle differences within the BMO's electronic structures, such as different band-gaps and different offsets of the valence band tops. The latter are found to be caused not by the influence of the M ion electronic states, but by particular behavior of the M–O and the Bi–O chemical bonds. © *2011 American Institute of Physics*. [doi:10.1063/1.3652751]

I. INTRODUCTION

The family of crystals with sillenite structure and chemical formula $Bi_{12}MO_{20}$ (BMO, with M = Ti, Ge, and Si) has attracted significant scientific attention for decades, mostly because of its pronounced photorefractive effect that is used in many applications: multi-wavelength holography,[1] real-time holographic surface imaging,[2] holographic imaging and interferometry,[3] and a variety of photocatalytic applications.[4–6] Although the members of the family, $Bi_{12}TiO_{20}$ (BTO), $Bi_{12}GeO_{20}$ (BGO), and $Bi_{12}SiO_{20}$ (BSO), are isostructural (space group *I*23) and have quasi-identical chemical composition (differing by just one atom in the 33-atom unit cell), they do not exhibit identical optical characteristics. Compared to BGO and BSO, the BTO presents higher photosensitivity to the red light, a higher electro-optical coefficient (linearly related to photorefractive sensitivity), and lower optical activity (which improves self-diffraction during hologram formation).[7–9] It thus presents some advantages over the BGO and BSO for the applications which explore the photorefractive effect. From these facts, it follows that optical characteristics (especially magneto-optical) of BMOs depend on the nature of the M ion, but this dependence is not simply traceable. As the optically active center in the BMOs is the Bi, the role of the M ion is limited to influence the situation in the Bi surrounding (its geometry, Bi–O distances, and electronic structure) in such a way which results in observable differences in photorefractive properties. Clarification of this influence is additionally complicated by the fact that photorefractive properties are usually defect dependent, and all of the"nominally pure" BMOs usually contain a significant amount of various intrinsic defects.[10–12] It is thus of great interest to describe the properties of perfect sillenite crystals, mostly for two reasons: (1) to be able to recognize which characteristics originate from the defects and which from the ideal crystal and (2) to predict possible changes of their properties in desirable directions.

So far, the structural, electronic, and optical properties of sillenites have been extensively studied experimentally (see Refs.13 and 14 and references therein), but very poorly theoretically. First electronic structure results of the BGO and BSO have been shortly discussed in Ref. 15, where the authors performed cluster calculations based on local pseudopotential method with various parameters extracted from fitting the experimental curves. In Ref. 16, the electronic structure of the BGO is calculated by the relativistic DV-Xα method. First-principles pseudo-potential calculations have been performed on the pure BTO in Refs. 17 and 18, but with controversial results about its band structure. This issue has been resolved in recent publications of our group,[19] where we calculated band structure and complex dielectric tensor of the BTO using the full-potential linearized augmented plane waves (FP-LAPW)[20] with generalized gradient approximation of Perdew-Burke-Ernzerhof (GGA-PBE)[21] for the exchange and correlation potential. Neither of the above cited works has discussed optical and magneto-optical properties of sillenites, except the last mentioned one, which dealt with the linear optical response of the BTO only.

The first objective of this paper is to accurately determine the structural, electronic, optical, and magneto-optical properties of pure sillenites and gather all these theoretical data at one place. Our second objective is to compare obtained results for each compound and search for differences that might be responsible for their different optical characteristics. Toward these goals, we performed identical *ab initio* density-functional theory (DFT)[22] based calculations on three pure BMO compounds, utilizing the most advanced and up-to-date tools for describing exchange and correlation effects between electrons: GGA-PBE for structural investigations (lattice and atom relaxations) and recently developed modified Becke-Johnson (mBJ) potential[23] for band-structure and optical calculations. The latter potential has

a)Electronic mail: mlalic@ufs.br.

been proven to cure some of the DFT deficiencies and provide better agreement of the calculated bandgap values and optical properties with the experimental data, at least for a large class of tested insulators.[23–25] Details of calculations are presented in Sec. II, obtained results are systemized and discussed in Sec. III, and conclusions are summarized in Sec. IV.

II. CRYSTAL STRUCTURE AND CALCULATIONS DETAILS

The crystal structure of the BMOs is body-centered cubic, with the space group *I23* (n° 197). The prototype compound is a mineral sillenite, γ-Bi_2O_3, which is metastable at ambient conditions. The two basic building blocks of crystal structure are usually considered to be the $(BiO_7)^{11-}$ polyhedrons interconnected in a complex manner (see details in Ref. 14) and the $(MO_4)^{4-}$ tetrahedrons situated at the corners and the center of the conventional unit cell, as shown in Fig. 1. The Bi atoms occupy the 24*f* and the tetravalent M atoms the 2*a* Wyckoff positions. The oxygen atoms are situated in three nonequivalent crystallographic sites, O(1) at the position 24*f* and O(2) and O(3) at the position 8*c*. The primitive unit cell contains one formula unit (33 atoms) without having a center of inversion.

The self-consistent calculations of the BMOs were performed by full potential linear augmented plane wave (FP-LAPW) method,[20] based on density-functional theory (DFT)[22] and implemented in the WIEN2k computer code.[26] In this method, the electronic wave functions, charge density, and crystal potential are expanded in spherical harmonics inside the non-overlapping spheres centered at each nuclear position (atomic spheres) and in plane waves in the rest of the space (interstitial region). The choice for atomic sphere radii was 2.3 for Bi, 1.8 for M, and 1.4 for O (in atomic units). Inside atomic spheres, the partial waves were expanded up to $l_{max} = 10$, while the number of plane waves in the interstitial was limited by the cut-off at $K_{max} = 7.0/R_{MT}$. As a basis set, the augmented plane waves were used. The charge density was Fourier expanded up to $G_{max} = 14$. A mesh of 7 k-points in the irreducible part of the Brillouin zone was used. The Bi 5*d*, 6*s*, 6*p*, the O 2*s*, 2*p*, the Ti 3*s*, 3*p*, 4*s*, 3*d*, the Ge 3*d*, 4*s*, 4*p*, and the Si 3*s*, 3*p* electronic states were considered as valence ones and treated within the scalar-relativistic approach, whereas the core states were relaxed in a fully relativistic manner. Exchange and correlation effects were treated in a two-fold manner. The relaxation of each of the BMO's crystalline structure has been performed using the generalized gradient approximation with Perdew-Burke-Ernzenhof parameterization (GGA-PBE).[21] Then, for each of the relaxed crystal structures, electronic bands and optical response have been calculated using the semi-local modified Becke-Johnson (mBJ) functional of Tran and Blaha.[23] The spin-orbit coupling has been taken into account just for heavy Bi atoms via a second variational procedure, using scalar-relativistic eigenfunctions as a basis. The self-consistent calculations for all three sillenites were performed on the same level of precision and all were successfully converged within the energy precision of 10^{-5} Ry.

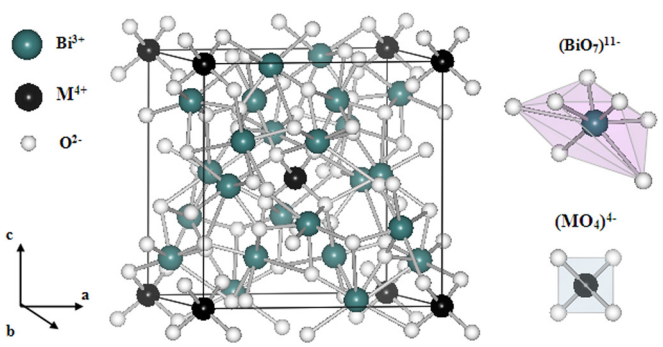

FIG. 1. (Color online) Crystal structure of $Bi_{12}MO_{20}$ (M = Ti, Ge, Si). Each Bi^{3+} ion is considered to be surrounded by 7 O's ions forming a $(BiO_7)^{11-}$ distorted polyhedral, while each M^{4+} ion is coordinated by 4 O's ions arranged in a $(MO_4)^{4-}$ perfect tetrahedron.

After their electronic structures had been determined, the linear optical properties of sillenites were computed using the WIEN2k optical package.[27] This package firstly calculates the imaginary part of the complex dielectric tensor ε_2, which is directly proportional to the optical absorption spectrum of the material, on the basis of the following formula:[28]

$$\varepsilon_{2(\alpha\beta)}(\omega) = \frac{4\pi^2 e^2}{m^2\omega^2}\sum_{i,f}\int_{ZB}\frac{2dk}{(2\pi)^3}|\langle\varphi_{fk}|P_\beta|\varphi_{ik}\rangle|| \times \langle\varphi_{fk}|P_\alpha|\varphi_{ik}\rangle|\delta[E_f(k) - E_i(k) - \hbar\omega]. \quad (1)$$

The formula (1) is valid in the limit of linear optics with electron polarization effects neglected and within the frame of random phase approximation. It describes electric dipole allowed transitions from populated Kohn-Sham states $|\varphi_{ik}>$ of energy $E_i(k)$ to empty Kohn-Sham states $|\varphi_{fk}>$ of energy $E_f(k)$ with the same wave vector k (ω is the frequency of the incident radiation, m the electron mass, P the momentum operator, and α and β stand for the projections x, y, or z). The ε_2 is computed up to an incident radiation energy of $\hbar\omega = 40$ eV with a mesh of 45 k-points in the irreducible wedge of the first Brillouin zone. The real part of the dielectric tensor ε_1 is then calculated using Kramers–Kronig relations. The knowledge of $\varepsilon(\omega) = \varepsilon_1(\omega) + i\varepsilon_2(\omega)$ permits calculation of various optical properties (refractive index, reflectivity, optical conductivity, etc.), which characterize the propagation of the electromagnetic wave through the material. Owing to the cubic symmetry of the sillenites, their dielectric tensors are diagonal, with $\varepsilon_{xx} = \varepsilon_{yy} = \varepsilon_{zz} = \varepsilon$, and thus reduced to scalar functions $\varepsilon(\omega)$.

The information about magneto-optical (MO) properties of material can also be accessed from the complex dielectric tensor.[27] Namely, optically active materials are characterized by appearance of the small non-diagonal components of its dielectric tensor, even if their crystal structure is cubic. In the case of sillenites, the MO effect arises principally from the strong spin-orbit coupling on the Bi atoms, which breaks the symmetry between left- and right-hand circularly polarized light and leads to different refractive indices for these two types of polarizations. If the magnetization direction, established by SO coupling, is taken to be along the z-axis and parallel to the direction of light propagation, there appears a non-zero off-diagonal component ε', which couples

the x- and y-components of the optical electric field, and the dielectric tensor takes the following form:

$$\boldsymbol{\varepsilon} = \begin{bmatrix} \varepsilon & \varepsilon' & 0 \\ -\varepsilon' & \varepsilon & 0 \\ 0 & 0 & \varepsilon \end{bmatrix}.$$

All tensor components are complex quantities: real parts $(\varepsilon_1, \varepsilon_1')$ describe dispersive and imaginary parts $(\varepsilon_2, \varepsilon_2')$ describe absorptive behavior of the material. As a consequence, incident, linearly polarized light is transmitted through the material, with its polarization plane perturbed by a complex angle $\theta(\omega)$, approximately given by[29]

$$\theta(\omega) = \frac{\pi}{\lambda}\frac{\varepsilon'}{\sqrt{\varepsilon}}, \tag{2}$$

where $\varepsilon' \ll \varepsilon$ and λ is the incident light wavelength. A real part of θ describes the angle by which the polarization axis of incident light is rotated when it passes through the unit length of the material. It is called specific Faraday rotation or optical rotatory power (θ_F):

$$\theta_F(\omega) = \frac{\pi}{\lambda}\frac{n\varepsilon_1' + k\varepsilon_2'}{n^2 + k^2}. \tag{3}$$

The imaginary part of θ, called Faraday ellipticity or magnetic circular dichroism (η_F), is given by

$$\eta_F(\omega) = \frac{\pi}{\lambda}\frac{n\varepsilon_2' - k\varepsilon_1'}{n^2 + k^2} \tag{4}$$

and describes the difference between the absorption of right- and left-handed circularly polarized light per unit length of the material. In formulas (3) and (4), the n and k are refractive index and extinction coefficient, respectively.

III. RESULTS AND DISCUSSION

A. Computation optimization and structure investigation

We started our calculations with a full optimization of the BMO's crystal structures. Both lattice parameters and atomic positions within unit cells were relaxed in order to reach values which correspond to energy minimum in our computer simulations. The relaxation of lattice parameters resulted in a = 10.322 Å for the BTO,[19] a = 10.469 Å for the BGO, and a = 10.387 Å for the BSO. These values are to be compared to experimentally determined a = 10 188 Å (BTO),[30] a = 10 145 Å (BGO),[31] and a = 10 104 Å (BSO).[31] They correspond to 4% (BTO), 10% (BGO), and 9% (BSO) larger unit cell volumes than determined by experiments[30,31] realized at ambient temperature. An increase of the theoretical volumes is expected, since the GGA tends to expand lattice constants in comparison with the experimental values.[32] Nevertheless, this expansion is surprisingly high for the BGO and BSO. As the next step, all atomic positions inside the relaxed unit cells were optimized by moving the atoms according to forces which act on them (using damped Newton scheme)[33] and obeying the symmetry constraints of the space group. The procedure has been repeated until forces became less than 2.0 mRy/a.u for all atoms.

The objective of structural relaxation was three-fold: (1) to obtain the equilibrium atomic positions to be used for electronic structure and optical calculations, (2) to test the reliability of the computational method, and (3) to compare local structures around Bi and M ions, searching for the differences that might be responsible for different optical characteristics of the BMO's.

While the coordination of the M^{4+} ions is regular (perfect tetrahedron with 4 O(3) at its vertices), the typical local structure around the Bi^{3+} ions is usually considered to consist of 7 O's, all situated at different distances, forming an irregular polyhedron around the Bi (Fig. 2, left). There are four oxygens situated in the equatorial plane (O(1b), O(1c), O(3), and O(2)), one in the apical position on one side of this plane (O(1a)), and two on the other side of the plane (O(1d) and O(1e)). Results of our computational optimization confirmed this arrangement for all BMO's (Fig. 2, on the right), but with one additional oxygen O(2)' situated within the polyhedron. This oxygen was initially separated from the Bi by 3.587 Å in the BTO, 3.543 Å in the BGO, and 3.488 Å in the BSO (experimental structures), but has approached to it during the relaxation process.

Tables I and II summarize all calculated BMO's lattice constants, interatomic distances, and angles in the Bi- and M-ion first coordination spheres and confront them with the corresponding experimental data. The tables demonstrate good overall agreement between calculated and experimental data. There can be noticed just two significant discrepancies: (1) the appearance of one additional oxygen atom within the

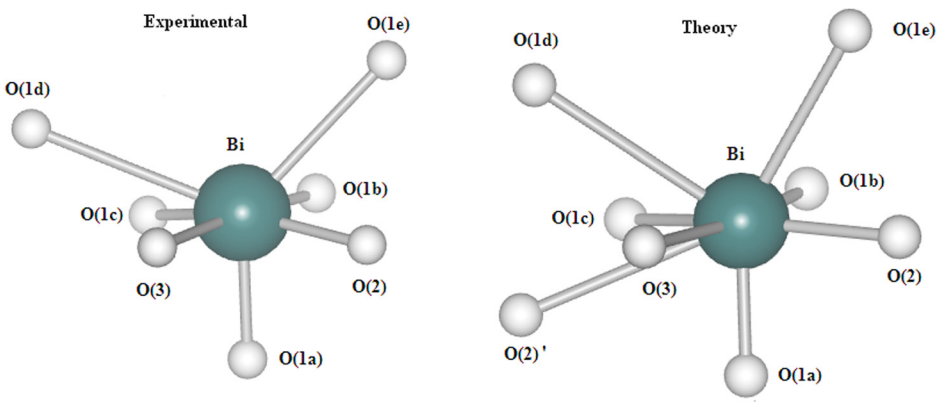

FIG. 2. (Color online) The local structure around the Bi ions in the BTO. Left: the structure determined on the basis of reported experimental data (Ref. 30), taken as a starting point in our calculations. Right: the resulting theoretical structure after computational optimization. A very similar situation is found for the BGO and BSO and therefore not shown here.

TABLE I. Calculated equilibrium lattice constants and interatomic distances (in Å) in the BTO, BGO, and BSO compared to experimental data.

	BTO		BGO		BSO	
	Theory[a]	Expt.[b]	Theory[c]	Expt.[d]	Theory[c]	Expt.[d]
a	10.322	10.188	10.469	10.145	10.387	10.104
Bi–O(1a)	2.063	2.163	2.048	2.076	2.042	2.064
Bi–O(2)	2.234	2.205	2.233	2.228	2.241	2.201
Bi–O(1b)	2.304	2.206	2.305	2.220	2.313	2.222
Bi–O(1c)	2.592	2.514	2.647	2.623	2.657	2.621
Bi–O(3)	2.788	2.622	2.871	2.640	2.871	2.647
Bi–O(1d)	2.968	3.131	3.081	3.082	3.059	3.066
Bi–O(2)′	3.205	3.587	3.225	3.543	3.176	3.488
Bi–O(1e)	3.352	3.370	3.456	3.170	3.494	3.161
M–O(3)	1.842	1.809	1.812	1.717	1.680	1.647

[a]Reference 19.
[b]Reference 30.
[c]This work.
[d]Reference 31.

TABLE II. Calculated equilibrium interatomic angles (°) within the Bi polyhedron in the BTO, BGO, and BSO crystals compared to experimental data.

	BTO		BGO		BSO	
	Theory[a]	Expt.[b]	Theory[c]	Expt.[d]	Theory[c]	Expt.[d]
O (1a)–Bi–O (2)	82.5	81.0	85.6	80.8	85.7	81.2
O (1a)–Bi–O (1c)	92.7	81.9	93.8	84.4	93.7	84.2
O (1a)–Bi–O (3)	82.5	88.4	83.7	85.5	84.4	86.4
O (1a)–Bi–O (1b)	101.5	88.1	103.8	91.2	103.0	91.0
O (1a)–Bi–O (1e)	124.2	113.4	123.6	114.0	124.3	114.0
O (1a)–Bi–O (1d)	146.8	134.7	149.6	138.3	150.1	138.3
O (1b)–Bi–O (1c)	59.8	64.8	58.7	68.7	57.8	68.3
O (2)–Bi–O (3)	99.0	86.2	98.13	85.9	98.4	83.9
O (2)–Bi–O (1b)	86.7	91.7	88.0	86.1	85.7	87.4
O (1d)–Bi–O (1e)	85.1	116.7	82.9	107.4	81.8	107.3
O (1c)–Bi–O (3)	115.3	116.2	116.0	118.6	119.0	119.6
O (2)–Bi–O (1c)	144.6	151.3	145.6	150.2	142.4	151.4
O (1b)–Bi–O (3)	173.5	176.1	170.7	171.7	171.8	171.2

[a]Reference 19.
[b]Reference 30.
[c]This work.
[d]Reference 31.

Bi polyhedron in the theoretical structure and (2) considerably smaller theoretical interatomic angles O(1d) – Bi – O(1e) in all 3 BMO's.

Comparing the local structures around the Bi^{3+} ions in the BMO's (either theoretical or experimental ones), one cannot notice significant difference. Although the interatomic distances and angles are not completely equal, they are very similar and the oxygen atoms are arranged in the same manner around the Bi. On the other hand, the first coordination sphere of the M ion is influenced by the ion-type in their respective materials. This should be related to the decreasing ionic radii of the M atoms going from the Ti to the Si: Ti^{4+} (0.68 Å), Ge^{4+} (0.53 Å), and Si^{4+} (0.26 Å). The M–O(3) distances clearly follow the same trend.

B. Electronic structure

The BMO's electronic band structures in the vicinity of their fundamental gaps are shown and compared in Fig. 3. It is seen that the overall dispersion of energy bands along high-symmetry directions of the Brillouin zone is quite similar in all three compounds. The other common fact is that all BMO's are direct band-gap materials, since their valence-band maxima and conduction-band minima are both located at the Γ point. The band structures in Fig. 3, however, exhibit two important differences. The first of them concerns the dispersion and relative position of the group of bands situated at the very top of the valence panel. These bands originate from the 2*p* states of O(3). In the BTO, these bands are more dispersed and more adhered to the lower-energy valence bands than in the BGO and, especially, BSO. The second difference concerns the different band gaps of the BMO's: 3.30, 3.04, and 2.85 eV for the BTO, BGO, and BSO, respectively. This result does not agree with experimental findings that all three nominally pure BMO's have the same gap, with a value between 3.20 and 3.28 eV.[34–36] The gaps calculated in this work are, however, closer to experimental ones than the gaps calculated earlier (2.3 eV[19] and 2.6 eV[17] for the BTO and 2.8 eV[15] for the BGO and

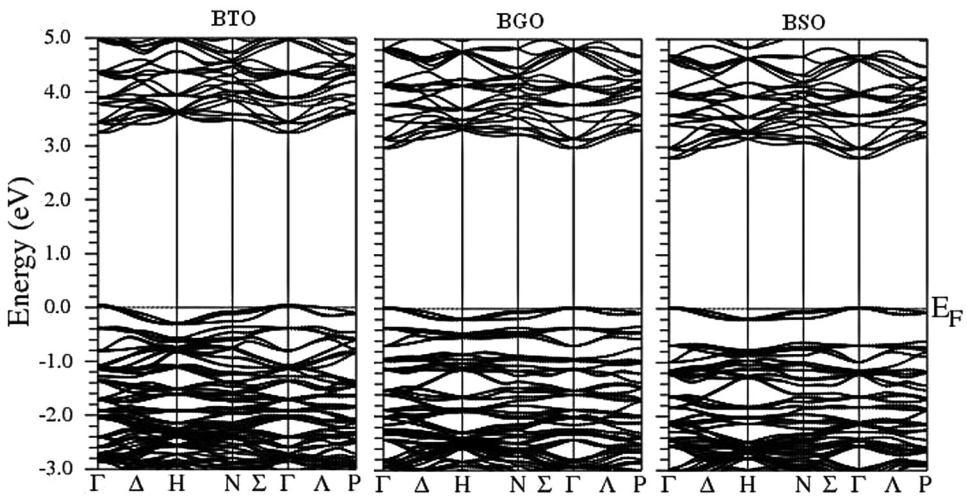

FIG. 3. Calculated energy band structures in the vicinity of fundamental bandgap of the BTO (left), BGO (middle), and BSO (right) crystals along the high-symmetry directions in the first Brillouin zone. Dot line indicates the Fermi level.

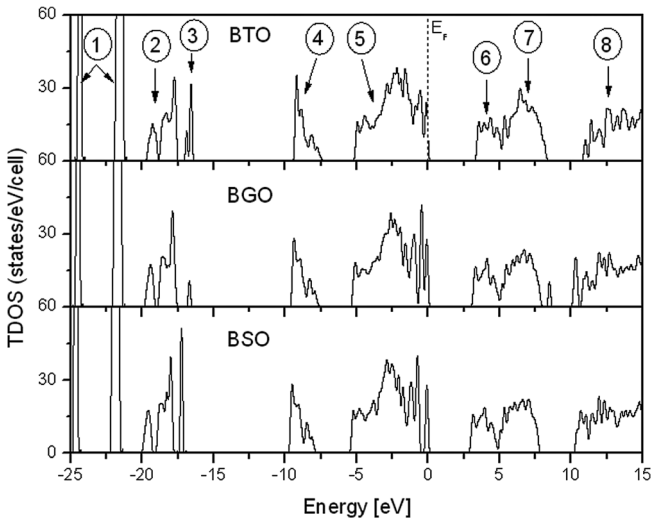

FIG. 4. Calculated total density of states (TDOS) of the BTO (top), BGO (middle), and BSO (bottom). Numbers 1-8 denote blocks of electronic states whose orbital character is described in the text. Dot line indicates the Fermi level.

BSO). This is a merit of usage of the recently developed mBJ exchange-correlation functional,[23] which has been tested to significantly improve gaps in a large class of insulators.[24,25] We also performed the electronic structure calculations of the BMOs using the GGA-PBE functional and obtained very similar band offsets, as shown in Fig. 3, but with the bandgap values of 2.30, 2.08, and 1.91 for BTO, BGO, and BSO, respectively.

In order to obtain more detailed insight into the BMO's electronic structure, we calculated the total and partial densities of electronic states (TDOS and PDOS) and show them in Figs. 4 and 5. The TDOS (Fig. 4) reveals a similarity of the electronic density of states in three materials. The TDOS is formed of five blocks of states in the valence region (identified by numbers 1 to 5) and three blocks of states in the conduction region (6 to 8). The blocks 1, 2, 4, and 6 present no significant differences in all three compounds. They are formed mainly by the Bi 5*d*, the O's 2*s*, the Bi 6*s*, and the Bi

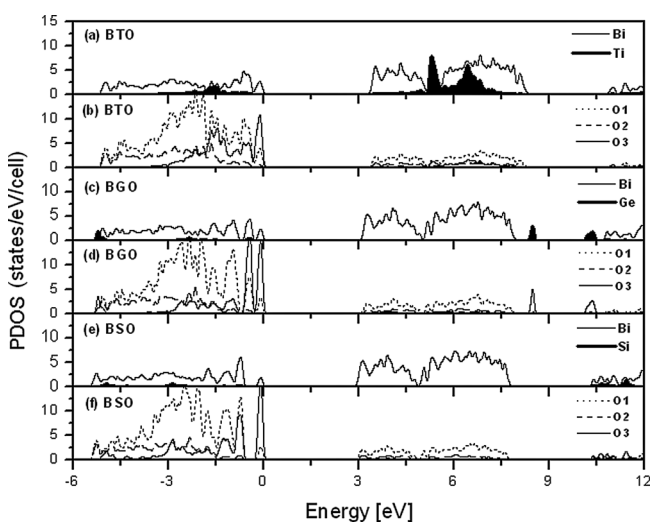

FIG. 5. Calculated partial density of states (PDOS) of the BMO's in the energy interval which comprises blocks of states 5-7 defined in Fig. 4.

6*p* states, respectively. The block 8 also has similar character in all three sillenites. It consists of a mixture of many states and cannot be clearly attributed to any particular state of any particular atom. The other blocks, however, present particularities. The block 3, for instance, is composed of the Ti *s* and *p* states in the BTO, the Ge *p* states in the BGO, and the Si *p* states in the BSO. It is, therefore, formed exclusively from the M ion's states. The origin of the more complex blocks 5 and 7 must be analyzed with the aid of Fig. 5.

According to Fig. 5, the block 5 is dominated by the 2*p* states of all three types of O's, but also has significant contribution of the Bi 6*s* and 6*p* states. Besides, this block has a small contribution of the Ti 3*d* (BTO), the Ge 4*p* (BGO), and the Si 3*p* states (BSO). The highest energy peak of this block is dominated by the 2*p* states of the O(3) hybridized with the 6*s* states of the Bi. It is interesting to note that the Bi $6s^2$ lone pair concentrates its states in two distinct energy regions: bonding ones are situated within block 4 and nonbonding ones are spread over block 5, but especially concentrated at its highest energy peak. This situation is quite similar to the situation that occurs in the $Bi_4M_3O_{12}$ eulytine compounds.[37] The O(3) coordinate the M ions, but also appear in the first coordination sphere of the Bi (see Table I), serving as a bridge between the BiO_8 and the MO_4 structures. They are thus bonded to both the Bi and the M ion at the same time. The O(3) are situated farthest from the M ion and nearest to the Bi ion in the BTO compound. In the BGO and especially the BSO, the M–O(3) bond is shorter and the Bi–O(3) bond longer. Being hybridized with the M and the Bi states, the energy of the O(3) states strongly depends on the M–O(3) and Bi–O(3) distances. The shorter M–O(3) distance favors the oxygen bonding with the M ion, increasing, at the same time, the energy of the bond with the Bi. This effect causes detachment of the hybridized Bi 6*s* and the O(3) 2*p* states from the very top of the valence bands in the BGO and the BSO compounds (Figs. 3 and 5).

Finally, the block 7 is mainly composed of the Bi 6*p* states in all three materials. In the BTO, however, this block contains significant amount of the Ti 3*d* states (Fig. 5(a)), contrary to the cases of the BGO and BSO, where no Ge or Si states appear in that energy interval (Figs. 5(c) and 5(e)). In the BGO, the Ge empty 4*p* states are distributed within two isolated small peaks centered at 8.5 and 10 eV, approximately, while in the BSO, the Si empty states appear even at higher energies.

C. Linear optical response

Figure 6 shows the calculated imaginary part of the dielectric function ε_2 of the three BMO's as a function of incident radiation energy in the range of 0−35 eV. The ε_2 is interpreted in terms of the BMO's electronic structures, presented in Figs. 4 and 5. All three absorption spectra have very similar forms, although their starting edges are dislocated due to different band gaps of the compounds. Each spectrum consists of three principal broad structures. The lowest energy one, with highest intensity, covers the energy region from absorption edge to approximately 12 eV. It is followed by the medium energy structure, centered on

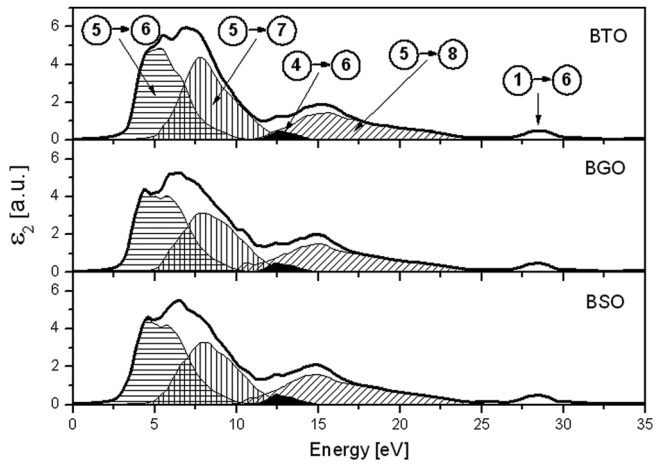

FIG. 6. Imaginary part of dielectric function of the BTO (top), BGO (middle), and BSO (bottom) crystals directly proportional to their optical absorption spectra as a function of incident radiation energy. The ε_2 is interpreted in terms of electronic transitions between the groups of bands defined in Fig. 4.

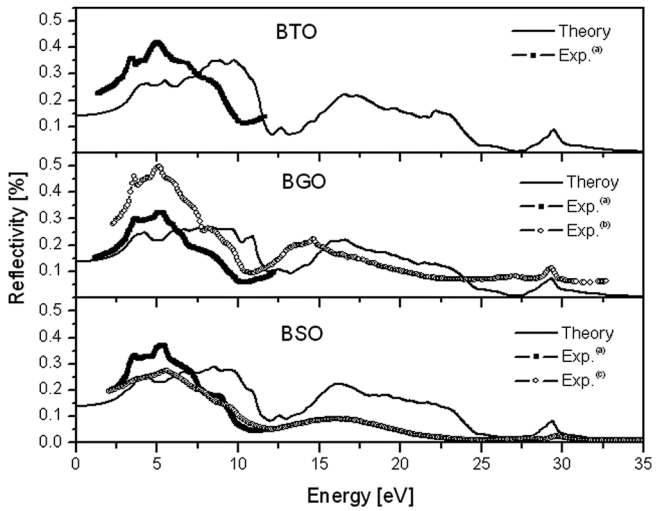

FIG. 7. The calculated reflectivity spectra of three sillenites. The experimental data (a) and (c) were taken from Ref. 14 and (b) from Ref. 16.

approx. 15 eV, which extends up to 25 eV. The third, high energy (and weak intensity) structure is situated between 27.5 and 30 eV.

Figure 6 demonstrates that all three absorption spectra can be interpreted in a similar manner (using a band characterization defined in Fig. 4). The low energy structure is formed by electronic transitions from block 5 to blocks 6 and 7. The first peak of this structure is caused by transitions from the O's 2*p* to the Bi 6*p* states and from non-bonding Bi 6*s* to the Bi 6*p* states, the latter being the less significant one. The same transitions are responsible for the formation of the second peak, but in the case of the BTO, there exists a significant contribution of the transitions from O's 2*p* to the Ti 3*d* states. This fact causes the slope of the BTO's low energy structure between 7.5 and 10 eV, slightly different in comparison to the BGO and BSO. The medium energy structure originates from transitions between block 4 and block 6 (from bonding Bi 6*s* to the empty Bi 6*p* states) and between block 5 and block 8 (from non-bonding Bi 6*s* and O's 2*p* to the hybridized states at higher energies). Finally, the high energy structure is caused by transitions from the occupied Bi 5*d* states (block 1) to the empty Bi 6*p* states (block 6).

Presented results demonstrate the importance of electronic transitions between the Bi and O within the BiO_8 polyhedron, which practically determine the form of optical absorption spectra in all three sillenites. On the other hand, electronic transitions between the M and O atoms within the MO_4 tetrahedron are of much less importance and occur at different energies for each respective compound: in the BTO between 5.5 and 10.5 eV, in the BGO between 8.5 and 13.5 eV, and in the BSO between 11.5 and 14.5 eV. These data partially support the discussion presented in Ref. 11, in which the authors estimate the energies of photons absorbed within the MO_4 tetrahedron as being 6.25 eV in the BTO and 8.75 eV in the BGO and BSO.

In order to confront our calculations with the experiment, which usually measures reflectivity and not absorption spectrum, we present in Fig. 7 the calculated BMO's reflectivity spectra along with available experimental data. Both theoretical and experimental BMO's spectra resemble each other as a consequence of similarity of their electronic structures. The BTO reflectivity spectrum, however, presents a slightly different intensity in the range of 7.5 to 10 eV in comparison to the BGO and BSO. This is due to significant participation of electronic transitions within the TiO_4 tetrahedron in this energy range, which is not observed within the corresponding MO_4 tetrahedrons in the other two sillenites. Agreement between the calculated and the experimental spectra is found to be good. The theory succeeded to predict the correct positions and widths of the 3 main broad peaks, thus reproducing the overall trend of the experimental spectra. The most significant discrepancy is found in the energy range from 7.5 to 10 eV, where the theoretical curve exhibits higher intensity than the experimental ones. Although we did not succeed in finding published experimental data for the BTO reflectivity in a far ultraviolet region, significant difference in comparison to the BGO and BSO data is not expected, due to similarity of the BMO's band structures.

D. Magneto-optical properties

Figure 8 presents calculated specific Faraday rotation for three BMO's in a visible wavelength range compared with available experimental data. The agreement between the theory and experiment is fair, especially for the long wavelengths. Additionally, calculations succeeded to reproduce correctly the experimental fact that the BTO's optical activity is significantly lesser that optical activities of BGO and BSO in a whole visible spectrum.

The situation is drastically changed when crystals are perturbed by ultraviolet light. In this case, our calculations predict that optical activity of the BTO should be larger than optical activities of BGO and BSO for most of the incident photon's energies (Fig. 9). This is especially true in the range between 3.5 and 5.5 eV, in which the Faraday angle for the BTO exhibits two broad structures (one positive and one negative). The quite similar conclusions can be drawn for respective Faraday ellipticities (Fig. 9).

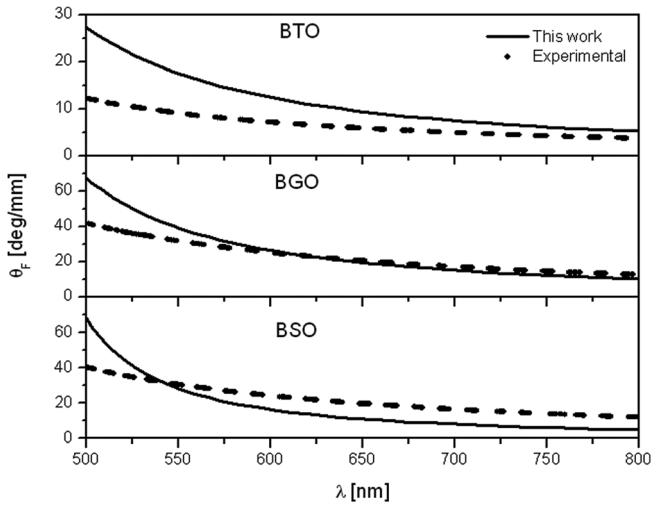

FIG. 8. Calculated optical rotatory power θ_F of three sillenites in a visible range. The magnitude of θ_F is a measure of optical activity: greater θ_F means larger activity and vice versa. The experimental data were taken from Ref. 7.

Figure 9 demonstrates very complex, oscillatory behavior for both optical rotatory power and Faraday ellipticity of all three BMO's. This behavior is difficult to interpret, having in mind that corresponding electronic structures (Figs. 3–5) are also very complex. In an attempt to explain why the BMO's exhibit different optical activities, some authors assume that electronic transitions within the BiO_8 polyhedron provoke clockwise Faraday rotation (positive angles), while those within the MO_4 tetrahedron have the opposite effect, i.e., provoke anti-clockwise Faraday rotation (negative angles).[11,12,14] This assumption is logically funded and enforced by some experimental evidences. It is, however, difficult to confirm it on the base of our theoretical investigation, mostly due to the fact that electronic states of the M ions are mixed with other electronic states. This means that the M–O(3) transitions occur simultaneously with the Bi–O transitions, making it impossible to evaluate their relative importance for each energy interval. There are, however, few exceptions. In the BTO, the first peak of the Ti empty d states, centered on 5.3 eV, is practically isolated from the Bi states (Fig. 5). The same can be concluded for the first peak of the Ge empty p states in the BGO, which is centered on 8.5 eV. In both compounds, the O(3) states are concentrated at the very top of the valence band at approx. 0 eV. Thus, we can be sure that transitions occurring at energies of 5.3 eV in the BTO and 8.5 eV in the BGO are largely composed of transitions within the MO_4 tetrahedron. Coincidently or not, exactly at these energies, the θ_F exhibits the most negative values in the BTO and BGO (Fig. 9). The other negative values of θ_F in the BMO's, however, can not be interpreted in the same way. Thus, at maximum, we dare to claim that our results allow a possibility that M–O and Bi–O transitions cause the opposite Faraday rotations.

Finally, according to formulas (2) and (3), the Faraday rotation is determined not only by a diagonal (ε), but also by a non-diagonal (ε') component of the dielectric tensor. The first component determines linear optical properties and the second magneto-optical properties of the materials. In order to discover which of these properties dominates the behavior of optical rotatory powers of the BMO's, we calculated ε_1,ε_2, ε'_1, and ε'_2 and compared them with θ_F and η_F within the range of 2−10 eV. The results and conclusions were found to be very similar for all three BMOs and, therefore, only one representative example is shown in Fig. 10 (θ_F for the BTO).

Figure 10 evidently shows that the oscillatory trend of the θ_F spectrum matches the oscillatory trend of ε'_1 almost perfectly, while at the same time, the ε exhibits slow and continuous changes in the same energy interval. Similar analysis of the η_F spectrum (not shown here) in the energy range of 2–10 eV demonstrates that the Faraday ellipticity is

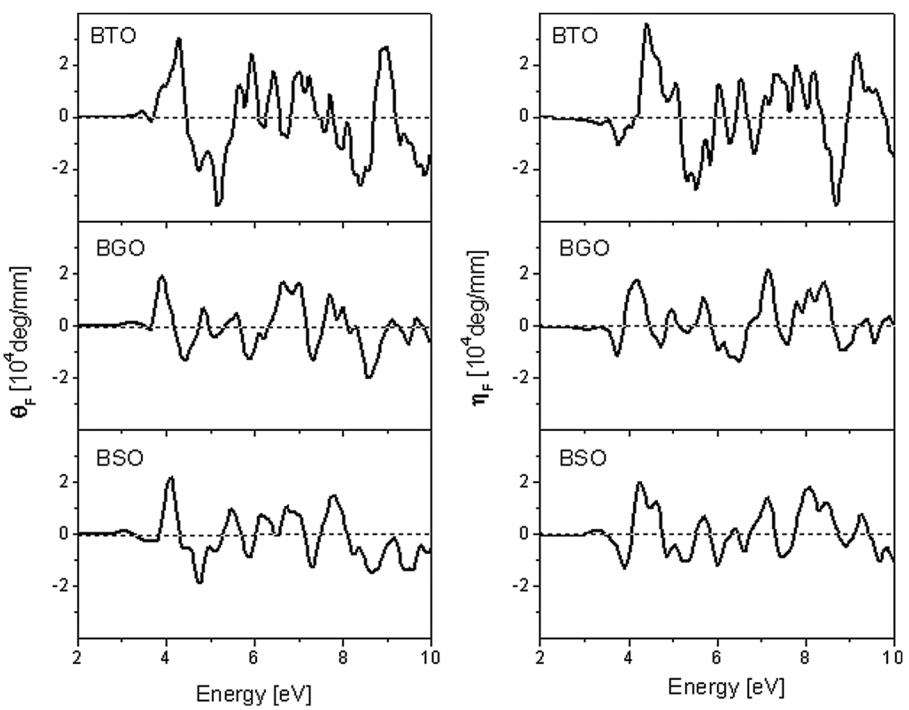

FIG. 9. Calculated optical rotatory powers and Faraday ellipticities of three sillenites in ultraviolet range.

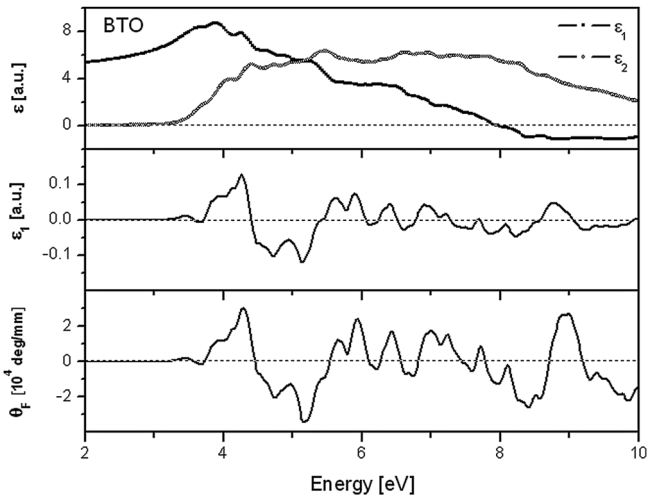

FIG. 10. Real and imaginary part of diagonal component of the BTO's dielectric tensor (top), real part of the off-diagonal component of the BTO's dielectric tensor (middle), and optical rotatory power spectrum of the BTO (bottom), all in the range of 2–10 eV.

totally governed by the ε_2' spectrum. Therefore, we can conclude that both θ_F and η_F sillenite spectra are completely determined by magneto-optical properties of the compounds.

IV. CONCLUSIONS

In this work, we presented a detailed comparative first-principles study of structural, electronic, optical, and magneto-optical properties of three sillenite compounds $Bi_{12}MO_{20}$ (BMO) (M = Ge, Si, and Ti) with the focus on differences that might be responsible for their different optical characteristics. The following principal conclusions have been reached:

1. The local structure around the Bi consists of 8 O's situated at the vertices of the irregular polyhedron around it. The arrangement of O's, including their distances and spatial positions, is found very similar in all three BMOs. The local structure around the ion M consists of the four equally distanced O's, which form a regular tetrahedron around it. The M–O distances are found to be very M-dependent.
2. The BMO's band structures, although generally very similar, exhibit three principal differences: (1) different bandgap values, (2) different forms of the valence band tops, and (3) slightly different forms of some parts of the conduction bands (especially at energies between 4.5 and 6.5 eV above the Fermi level). The first two differences are mainly caused by the detachment of the highest energy occupied states of the BGO and BSO from the rest of their valence bands. This process is shown to be provoked by different M–O(3) and Bi–O(3) bond lengths, where O(3) is the oxygen bonded to both the Bi and the M ions. The third difference arises mainly from a presence of abundant Ti empty *d* states within the BTO's conduction band, a fact which is not observed for the Ge and Si states in the BGO and BSO. The calculated bandgap values (in eV) are found to be 2.85 (BSO), 3.04 (BGO), and 3.30 (BTO) with the usage of mBJ XC-potential and 1.91 (BSO), 2.08 (BGO), and 2.30 (BTO) when the standard GGA-PBE XC-potential was used. Contrary to our results, experimental measurements indicate the same value of the bandgap in all three sillenites (3.20−3.28 eV). Although we cannot discard the possibility of error in our calculations (owing to usual DFT deficiencies), we must stress that, in our theoretical approach, we dealt with the perfectly pure crystal structure of sillenites. In reality, it is practically impossible to reach that structure due to various stoichiometric limitations during the crystal growth.[38] The experimental results, therefore, refer to nominally pure samples which contain a lot of intrinsic defects. Keeping this in mind, our study opens a possibility that the same experimental bandgap values of three BMO's might be provoked by the presence of intrinsic defects.
3. The linear optical properties of the BMOs in the ultraviolet range (absorption and reflection) are found to be practically identical and determined by electronic transitions that occur within the BiO_8 polyhedra. Electronic transitions within the MO_4 tetrahedra occur at higher photon's energies and do not visibly affect the forms of the absorption spectra. The only exception is the BTO, in which case the slope of the first broad absorption peak between the energies of 7.5 and 10.0 eV is slightly different compared to the BGO and BSO. This happens due to electronic transitions from the O's 2*p* states to the empty Ti 3*d* states within the TiO_4 tetrahedron, a fact which is not observed within the GeO_4 and SiO_4 tetrahedra in the BGO and the BSO.
4. The magneto-optical properties of the BMO's are found to be significantly different. Our calculations confirmed the fact that optical activity of the BTO is much lesser than optical activities of the BGO and the BSO in a visible spectrum. In the range of ultraviolet frequencies, however, the calculations predict a larger optical activity of the BTO in relation with the other two sillenites. The behavior of optical rotatory power and Faraday ellipticity of the BMOs is, however, very complex and hard to interpret. We have shown that this behavior has the magneto-optical origin, being caused by a non-diagonal component of the dielectric tensor. We also presented some indications that electronic transitions within the BiO_8 and the MO_4 polyhedra can cause the opposite Faraday rotations.

ACKNOWLEDGMENTS

The authors gratefully acknowledge the CNPq and FAPITEC-SE (Brazilian funding agencies) for financial support. We also thank Prof. Jaime Frejlich (UNICAMP – São Paulo) for fruitful discussions about the sillenites.

[1]E. A. Barbosa, R. Verzini, and J. F. Carvalho, Opt. Commun. **263**, 189 (2006).
[2]M. R. R. Gesualdi, D. Soga, and M. Muramatsu, Opt. Laser Technol. **39**, 98 (2007).
[3]E. A. Barbosa, A. O. Preto, D. M. Silva, J. F. Carvalho, and N. I. Morimoto, Opt. Commun. **281**, 408 (2008).
[4]C. He and M. Gu, Scr. Mater. **54**, 1221 (2006).
[5]W. F. Yao, H. Wang, X. H. Xu, J. T. Zhou, X. N. Yang, Y. Zhang, S. X. Shang, and M. Wang, Chem. Phys. Lett. **377**, 501 (2003).

[6]W. F. Yao, H. Wang, X. H. Xu, X. F. Cheng, J. Huang, S. X. Shang, X. N. Yang, and M. Wang, Appl. Catal. A Gen. **243**, 185 (2003).
[7]A. T. Efremidis, N. C. Deliolanis, C. Manolikas, and E. D. Vanidhis, Appl. Phys. B **95**, 467 (2009).
[8]J. P. Wilde and L. Hesselink, J. Appl. Phys. **67**, 2245 (1990).
[9]N. V. Kukhtarev, G. E. Dovgalenko, and V. N. Starkov, Appl. Phys. A **33**, 227 (1984).
[10]J. Frejlich, R. Montenegro, N. R. Inocente-Junior, P. V. Santos, J. C. Launay, C. Longeaud, and J. F. Carvalho, J. Appl. Phys. **101**, 043101 (2007).
[11]V. Marinova, Opt. Mater. **15**, 149 (2000).
[12]V. Tassev, M. Gospodinov, and M. Veleva, Opt. Mater. **13**, 249 (1999).
[13]J. Frejlich, R Montenegro, T. O. dos Santos, and J. F. Carvalho, J. Opt. A, Pure Appl. Opt. **10**, 104005 (2008).
[14]V. I. Burkov, A. V. Egorysheva, and Y. F. Kargin, Crystallogr. Rep. **46**, 312 (2001).
[15]I. V. Kityk, M. K. Zamorskii, and J. Kasperczyk, Physica B **226**, 381 (1996).
[16]M. Itoh, T. Katagiri, H. Mitani, M. Fujita, and Y. Usuki, Phys. Status Solidi B **245**, 2733 (2008).
[17]W. Wei, Y. Dai, and B. Huang, J. Phys. Chem. C **113**, 5658 (2009).
[18]J. Zhou, Z. Zou, A. K. Ray, and X. S. Zhao, Ind. Eng. Chem. Res. **46**, 745 (2007).
[19]A. F. Lima and M. V. Lalic, Comput. Mater. Sci. **49**, 321 (2010).
[20]O. K. Andersen, Phys. Rev. B **12**, 3060 (1975); D. J. Singh, *Plane Waves, Pseudopotentials and the LAPW Method* (Kluwer Academic, Dodrecht, 1994).
[21]J. P. Perdew, K. Burke, and M. Ernzerhof, Phys. Rev. Lett. **77**, 3865 (1996).
[22]P. Hohenberg and W. Kohn, Phys. Rev. **136**, B864 (1964); W. Kohn and L. J. Sham, Phys. Rev. **140**, A1133 (1965).
[23]F. Tran and P. Blaha, Phys. Rev. Lett. **102**, 226401 (2009).
[24]D. J. Singh, S. S. A. Seo, and H. N. Lee, Phys. Rev. B **82**, 180103 (2010).
[25]D. Koller, F. Tran, and P. Blaha, Phys. Rev. **83**, 195134 (2011).
[26]P. Blaha, K. Schwarz, G. K. H. Madsen, D. Kvasnicka, and J. Luitz, *An Augmented Plane Waves + Local Orbital Program for Calculating Crystal Properties* (Karlheinz Schwarz, Techn. Universität Wien, Austria, 2001).
[27]C. Ambrosch-Draxl and J. O. Sofo, Comput. Phys. Commun. **175**, 1 (2006).
[28]M. Bass, E. W. V. Stryland, D. R. Willians, and W. L. Woffe, *Handbook of Optics*, 2nd ed. (McGraw-Hill, New York, 1995), Vol. 1.
[29]P. Mihailovic, S. Petricevic, S. Stankovic, and J. Radunovic, Opt. Mater. **30**, 1079 (2008).
[30]Sh. M. Efediev, V. E. Bagiev, A. C. Zeinally, V. Balashov, V. Lomonov, and A. Majer, Phys. Status Solidi A **74**, 17 (1982).
[31]S. C. Abrahams, P. B. Jamieson, and J. L. Bernstein, J. Chem. Phys. **47**, 4034 (1967); S. C. Abrahams, J. L. Bernstein, and C. Svensson, J. Chem. Phys. **71**, 788 (1979).
[32]Z. Wu and R. E. Cohen, Phys. Rev. B **73**, 235116 (2006).
[33]B. Kohler, S. Wilke, M. Scheffler, R. Kouba, and C. Ambroseh-Drax, Comput. Phys. Commun. **94**, 31 (1996).
[34]S. L. Hou, R. B. Lauer, and M. L. Harvill, J. Appl. Phys. **44**, 2652 (1973).
[35]R. Oberschmid, Phys. Status Solidi A **89**, 263 (1985); B. C. Grabmaier and R. Oberschmid, Phys. Status Solidi A **96**, 199 (1986).
[36]V. M. Skorikov, I. S. Zakharov, V. V. Volkov, and E. A. Spirin, Inorg. Mater. **38**, 172 (2002).
[37]A. F. Lima, S. O. Souza, and M. V. Lalić, J. Appl. Phys. **106**, 013715 (2009).
[38]M. Valant and D. Suvorov, Chem. Mater. **14**, 3471 (2002).